Advances in Science and Technology Research Journal

Advances in Science and Technology Research Journal 2024, 18(1), 118–128
https://doi.org/10.12913/22998624/177029
ISSN 2299-8624, License CC-BY 4.0

Received: 2023.11.15
Accepted: 2023.12.15
Published: 2024.01.15

Influence of the Extrusion Cavity Shape on the Ultimate Extrusion Force Value During Pellet Extrusion through Multiple-Cavity Dies

Jan Górecki[1*], Wiktor Łykowski[1], Maria Gumeni[2]

[1] Faculty of Mechanical Engineering, Poznan University of Technology, ul. Piotrowo 3, 60-965 Poznań, Poland

[2] Faculty of Mechanical, Industrial and Transport Engineering, Chisinau, Technical University of Moldova, 9/8, Strada Studenților, Chișinău, Moldova

* Corresponding author's e-mail: jan.gorecki@put.poznan.pl

ABSTRACT

The article describes the results of experimental research that allowed us to compare the influence of the forming channel shape and its length on the limit value of the force occurring in the process of extruding crystallized carbon dioxide using multi-channel dies. To carry out the research, the authors adopted a method described in the literature, which allows for experimenting using a sublimating material under normal conditions, at a temperature of -78.4°C. Analysis of variance was used for the statistical analysis of the experiment results, which allowed to determine the level of statistical significance of differences between individual populations. Additionally, based on the median and regression values, an attempt was made to fit a function describing the change in the tested values as a function of geometric parameters. This allowed for comparison of the impact of individual variables. The authors did not observe the research results in the available literature, they would discuss the influence of the channel shape of multi-channel systems on the value of the confining force. Therefore, according to the authors, the presented results constitute an important supplement to the available knowledge.

Keywords: extrusion, compaction, dry ice, cavity shape, multichannel die.

INTRODUCTION

Transporting materials plays a vital part in the growth of civilisations. For centuries people have been looking for methods allowing to shorten the haulage time or increase the haulage distance. In the case of temperature-controlled goods, haulage technology developments must be accompanied by improvement of the associated storage methods. These temperature-controlled goods in transit include foodstuffs and medical products, in particular pharmaceuticals such as SARS COVID-19 vaccines with -80°C to -60°C [1] long-term storage temperature requirement. Dry ice shipping containers are one of the solutions to obtain these storage temperatures. Dry ice (DI) is solid carbon dioxide, in normal ambient conditions having a temperature of -78.4 °C [2]. As we see in the phase change diagram (Fig. 1), dry ice will sublimate in the said conditions. As it has been reported in earlier studies, sublimation adversely affects the cooling process efficiency [3].

Therefore, dry ice is generally subjected to mechanical processing, with the aim to improve its use efficiency. On industrial scale, special DI ram extruders are used for this purpose. The working system schematic is presented in Figure 2. The system of these machines has been extensively described by Górecki et al. 2019 [5]. Dry ice extrusion process consists of four subsequent stages. In the first stage, liquid carbon dioxide is injected into the compression chamber. This triggers an adiabatic process decreasing the material's temperature and changing its state from liquid to solid. In the next stage, the ram (2) moves along the compression chamber axis, thus compressing the initially loose material. This stage ends when the value of F_C has reached the value

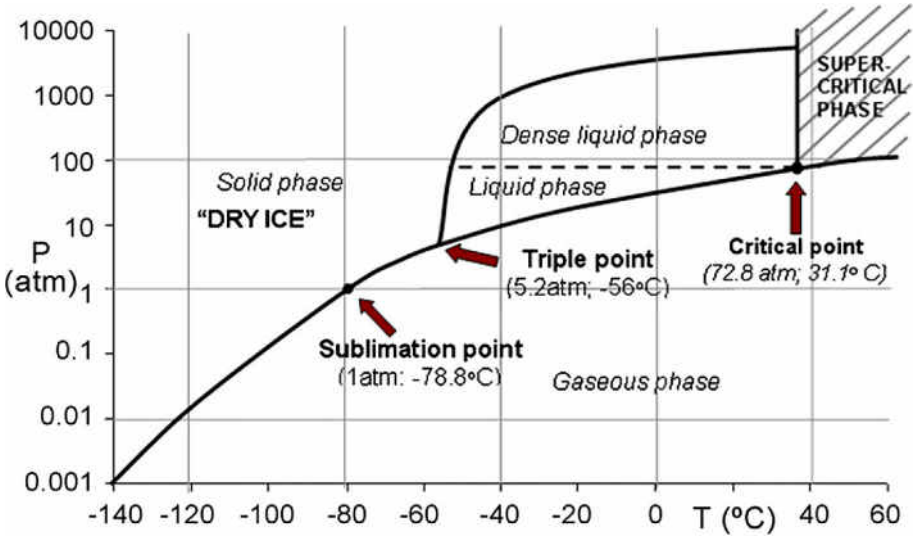

Figure 1. Phase diagram of CO_2 [4]

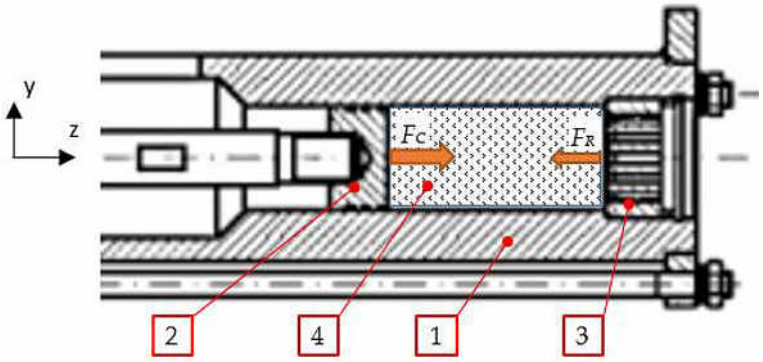

Figure 2. Extruder working system including multiple-cavity die, 1 – compression chamber, 2 – ram, 3 – multiple cavity die, 4 – loose dry ice, F_R – resisting force, F_C – compacting force [5]

of extrusion resistance force F_R. of the die in question, multiple-cavity type in this case. In the next stage compressed DI is pushed through the die cavity formed on the way to the pre-defined end-product shape, such as 3 mm pellets. As soon as the ram has reached the end-of-travel position, it is withdrawn to the home position and the cycle begins anew. The process of dry ice production been extensively described in the literature and the interested readers are advised to consult the referenced articles [6] for further details.

As mentioned, the purpose of this process is to reduce the material's surface area to reduce its sublimation rate. For this reason, the density of DI pellets ρ_{DI} [7] has been chosen as the extrudate quality indicator. Its value is directly related to the geometric features of multiple-cavity die (Fig. 3) and the billet length l_T before it gets split and extruded in the third stage of the process. In our earlier articles [8,9] we described the relationship between F_R and the geometric features of conical convergent multiple-cavity dies. The relevant geometric features of the analysed dies are shown in Figure 3. Wałęsa et al. (2022) presented the outcomes of a simulation study investigating the performance of single-cavity dies featuring four different convergent section geometries: conical, concave, convex and concave-concave, as shown in Figure 4. In the case of a constant value of the inlet diameter (D) and outlet diameter (d), the shape of the conic section determines the length of this section (h) or the convergence angle (α). For a spherical, convex, or concave convergent section, specify the radius value (R_1 or R_2) and the section's length (h_1 or h_2). In the case of the fourth type of channel, fixed from the connection of the two previous ones, it is necessary to determine the parameters for both sections independently or to ascertain the total length of the convergent section and define the proportion of each share, e.g.,

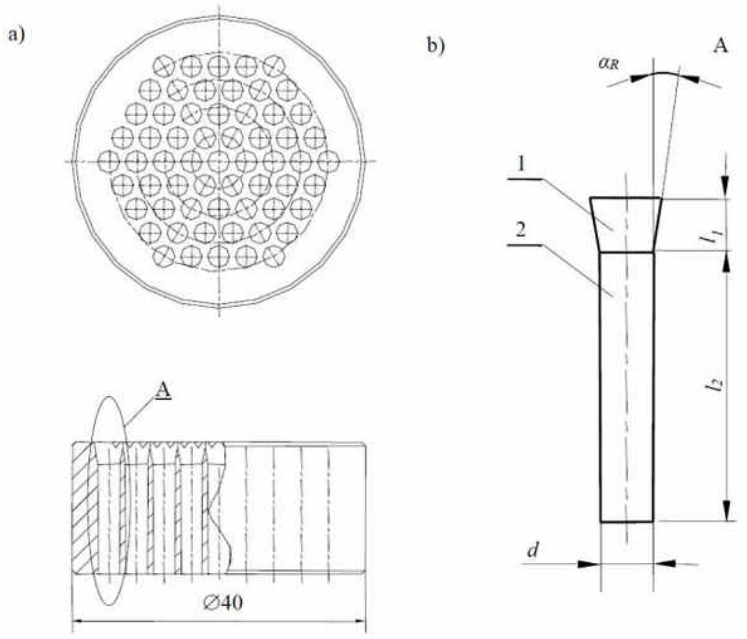

Figure 3. Conical convergent multiple-cavity die, (a*)* overview, (b) single cavity detail, *d* – die land diameter, α_R – side inclination of the conical section, l_C – conical section length, l_L – die land length [9]

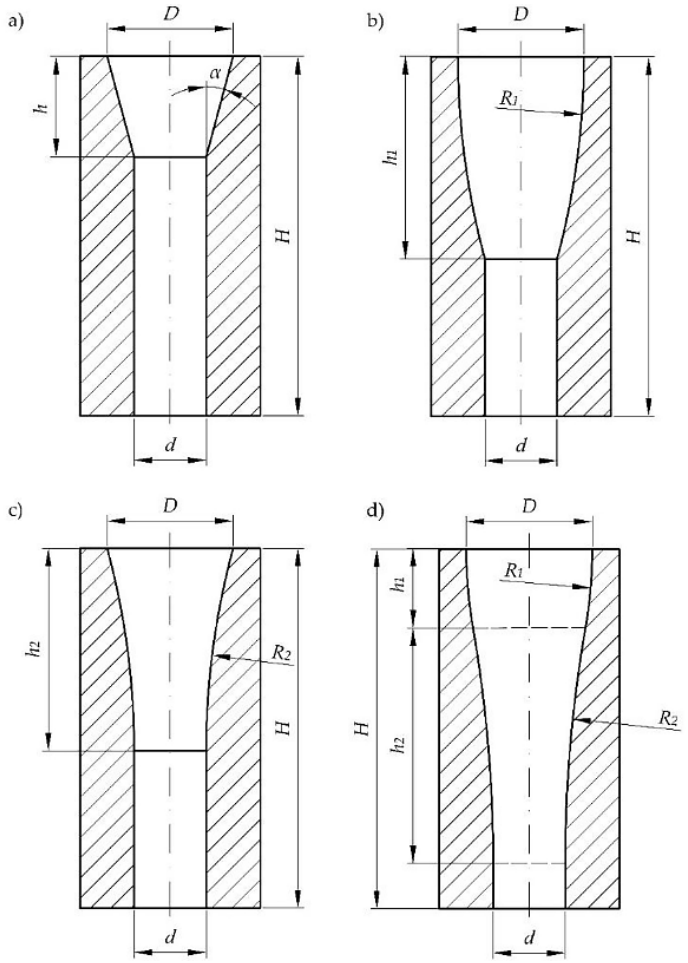

Figure 4. Shapes of the dies under analysis: (a) conical-cylindrical (CC), (b) with a convex spherical compression section, (c) with a concave spherical compression section (CS), (d) with a convex section followed by concave section (CCS) [13]

1 to 1. The convex spherical compression section was left out based on the results of earlier studies that revealed problems with obtaining laminar flow of the material during extrusion and maintaining cohesion. On the other hand, simulations with dies including a concave spherical compression section and a convex section followed by concave section showed that dies including a non-conical convergent section may be an option. This shows that the aforesaid shapes should be taken into consideration in research and development work on improving the efficiency of DI extrusion process using single-cavity dies.

The literature on the subject of multiple-cavity dies apparently does not include any reports on the effect of convergent sections shapes other than conical. In turn, the results presented in this article concern dies including convex and convex followed by concave convergent sections. Therefore, the article is intended to fill the revealed gap in knowledge. In addition, the said results may serve as reference data in DI extrusion numerical simulations using artificial intelligence techniques that are arousing great interest among machine design engineers of various fields [10-12].

METHODOLOGY AND MATERIALS

Materials

The material used in the experiments was loose dry ice of ca. 550 kg/m^3 bulk density [14]. It is obtained by expanding liquid carbon dioxide stored at -18 Celsius degrees from 20 bar to atmospheric pressure. The particle size of loose dry ice obtained in this way was determined by Liu et. al. 2010. It ranged 20–100 μm, depending on the method of expansion [15]. Figure 5 shows dry ice in different forms: loose (first from the left) and compacted into 3 mm pellets (second from the left) and 16 mm initial cross-section pellets (first from the right). The apparent non-cylindricity of the pellets results from the loss of material due to sublimation.

The dies

Multiple-cavity dies including CC, CS, and CCS convergent sections were used in the experiments. In each die type five different samples were prepared, featuring different convergent section lengths, ranging 1 mm to 9 mm. The geometric features of the analysed dies are shown in Figure 6, and the values are given in Table 1. For comparison purposes, the inlet diameter D , outlet diameter d, overall die length L and extrusion cavity layout remained the same between the tested dies. The experiments caused evident distortion of some cavities, and hence some h_c values were not included in Table 1.

Compression force measurement method

This study used the method described by Biszczanik et al. 2023, originally used to investigate the effect of geometric features of single-cavity dies on the DI extrusion process

Table 1. Geometric features of the analysed multiple-cavity dies

Die type			h_c [mm]		
CC	1	3	5	7	9
CS	1	3	5	7	9
CCS	1	3	5	7	9

Figure 5. Dry ice, from left to right: loose, 3 mm pellets, 16 mm pellets [16]

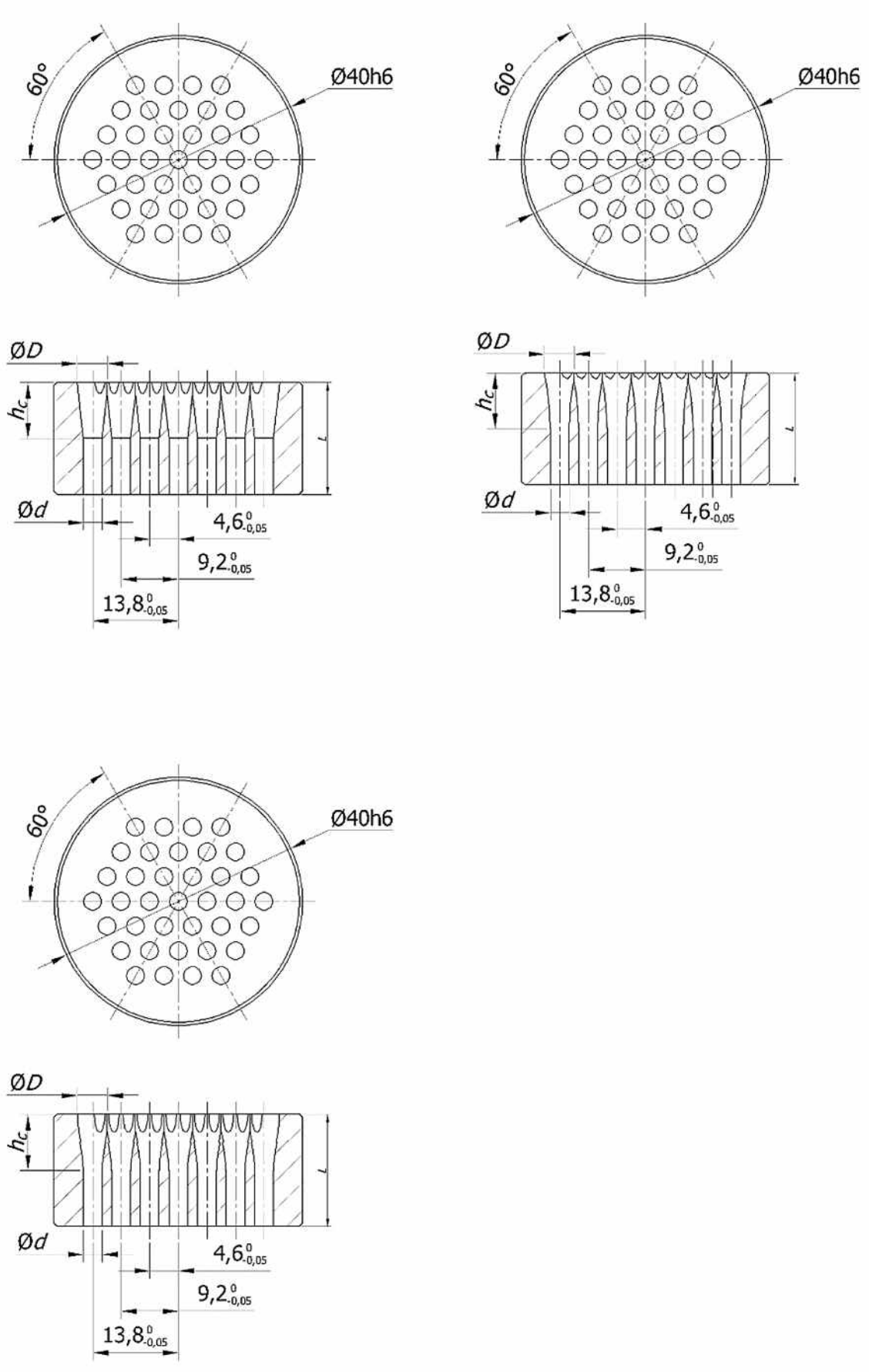

Figure 6. Multiple-cavity dies featuring the following convergent section types: (a) CC, (b) CS, (c) CCS, D equal to 5 mm, d equal to 3 mm, L equal to 18 mm

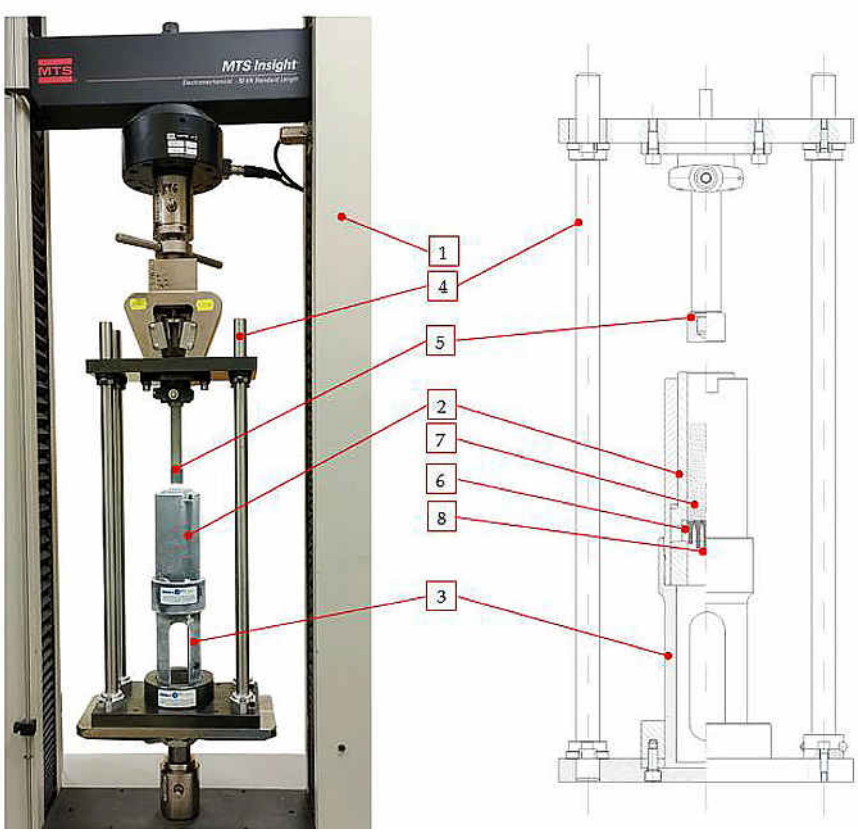

Figure 7. Dry ice compression and extrusion test facility, 1 – MTS Insight 50 kN test frame, 2 – Upper sleeve with the compaction chamber contained inside it, 3 – Lower sleeve, 4 – Guide assembly, 5 – Ram, 6 – Multiple-cavity die, 7 – Loose dry ice, 8 – Dry ice pellets

characteristics [16]. The experimental set-up is presented in Figure 7. This set-up allowed measurement of the applied force during the loose dry ice (Fig. 7, label 7) compression and extrusion stages, the extrudate being 3 mm pellets (Fig. 7, label 6), as defined by the parameter d of the applied multiple-cavity dies. In order to allow fitting of multiple-cavity dies (Fig. 7, label 6), the test set-up described by Biszczanik was modified to accommodate the greater compression chamber (Fig. 7, label 2) diameter of 38 mm and the associated increase in the ram diameter to 37.8mm (Fig. 7 label 3). The test facility was composed of MTS Insight 50 kN test frame (MTS Systems, USA, Eden Prairie) with the above-described test set-up mounted in the test frame grips. Dedicated TestWork 4.0 software by MTS Systems (USA, Eden Prairie) was used to control the test facility and log the measurement results with 50 Hz frequency. The linear motion of the top jaw pushes the top plate with the ram mounted thereon (Fig. 7, label 5) down at a speed of 5 mm/sec. This motion reduced the available space inside the compression chamber, resulting in compression of the material

Figure 8. The insulated dry ice storage container and the condition the experimental set-up components, 1 – insulated container, 2 – dry ice, 3 – experimental set-up [17]

contained therein (Fig. 7, label 7). The ram motion continued until it had reached the bottom end position located 1 mm above the top surface of the die. Next the ram was withdrawn to its home position and the next test cycle could begin. In order to reduce the effect of sublimation on the test results, all the parts that would get in contact with dry ice were pre-cooled. For this purpose, the sleeve assembly including the ram was placed in the DrIcy 30 firmy insulated dry ice pellet storage container manufactured by Melform of Monasterolo di Savigliano, Italy. The container containing the test set-up is shown in Figure 8. Each test series comprised three repetitions and the test set-up components were held in the insulated container for 30 minutes before the first series and then for 10 minutes in between.

RESULTS AND DISCUSSION

The following diagrams represents the change of compression force F_C as a function of ram displacement s obtained for CC die of h=5. The parameters measured to determine the effect of the geometric features for different convergent section types were the ultimate force F_C^{max} and the distance between the ram face and the multiple-cavity die $s(F_C^{max})$. The readings were logged as populations, in order to allow the use of the analysis of variance method (ANOVA) and determine the statistical significance value p of the hypotheses that the value of F_C^{max} had a bearing on:

- convergent section shape, irrespective of the section length (5 tests for h=const; type=var),
- convergent section length, irrespective of the section length (3 tests for type=const; h=var),
- convergent section surface area (1 test for S=var).

One-way analysis of variance along with Tukey post hoc test were used to assess the mean differences of F_C^{max} and ρ_{CCD} between the data groups. The analysis of data was performed using the Statistica software (Version 13.3, TIBCO Software Inc.). Statistical significance defined

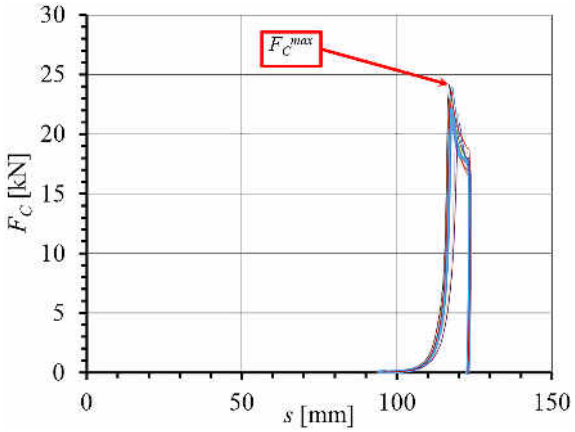

Figure 9. Change of F_C as a function of s: F_C^{max} – limit value of $F_C(s)$ during a trial

Table 2. Values of p between the compared populations for convergent section of CC shape

CC	h=3	h=5	h=7
h=3		0.000129	0.000129
h=5	0.000129		0.000129
h=7	0.000129	0.000129	

Table 3. Values of p between the compared populations for convergent section of CS shape

CS	h=3	h=5	h=7
h=3		0.003222	0.000130
h=5	0.003222		0.014358
h=7	0.000130	0.014358	

Table 4. Values of p between the compared populations for convergent section of CCS shape

CCS	h=3	h=5	h=7
h=3		0.000127	0.000127
h=5	0.000127		0.000127
h=7	0.000127	0.000127	

Table 5. Values of p between the compared populations for convergent section of h=3 mm

h=3	CC	CS	CCS
CC		0.000129	0.003899
CS	0.000129		0.000129
CCS	0.003899	0.000129	

Table 6. Values of p between the compared populations for convergent section of h=5 mm

h=5	CC	CS	CCS
CC		0.000134	0.000129
CS	0.000134		0.000129
CCS	0.000129	0.000129	

Table 7. Values of p between the compared populations for convergent section of h = 7 mm

h=7	CC	CS	CCS
CC		0.043723	0.000129
CS	0.043723		0.000129
CCS	0.000129	0.000129	

Table 8. Key descriptive statistics for verification of the effect of h on the value of F for the CC cavity shape

CC	AVR [kN]	Min. [kN]	Max. [kN]	Q25 [kN]	Q50 [kN]	Q75 [kN]
h=3	17. 11	16.04	18. 29	16.33	17.18	17.64
h=5	22. 62	19.15	24.11	22.12	22.93	23.97
h=7	33.00	29.17	34.72	33. 77	34.05	34.50

Table 9. Key descriptive statistics for verification of the effect of h on the value of F for the CS cavity shape

CS	AVR [N]	Min. [N]	Max. [N]	Q25 [N]	Q50 [N]	Q75 [N]
h=3	23.35	21.65	29.84	22.18	22.44	22.63
h=5	27.67	25.31	31.88	26.34	27.12	29.47
h=7	31.07	27.67	36.06	27.82	30.80	33.08

Table 10. Key descriptive statistics for verification of the effect of h on the value of F for the CCS cavity shape

CCS	AVR [kN]	Min. [kN]	Max. [kN]	Q25 [kN]	Q50 [kN]	Q75 [kN]
h=3	15.87	14.36	16.75	15.61	15.84	16.54
h=5	7.00	5.25	9.06	5.32	7.38	8.39
h=7	24.37	21.04	28.20	23.70	23.89	25.69

Table 11. Key descriptive statistics for verification of the effect of the convergent section shape on the value of F for h = 3 mm

h=3	AVR [kN]	Min. [kN]	Max. [kN]	Q25 [kN]	Q50 [kN]	Q75 [N]
CC	17.11	16.04	18.29	16.33	17.18	17.64
CS	22.54	21. 66	24.14	22.18	22.44	22.63
CCS	15.87	14.36	16.75	15.61	15.84	16.54

Table 12. Key descriptive statistics for verification of the effect of the convergent section shape on the value of F for h = 5 mm

h=5	AVR [kN]	Min. [kN]	Max. [kN]	Q25 [kN]	Q50 [kN]	Q75 [kN]
CC	22.62	19.15	24.11	22.12	22.93	23.97
CS	27.67	25.31	31.88	26.34	27.12	29.47
CCS	7.06	5.25	9.06	5.32	7.38	8.39

Table 13. Key descriptive statistics for verification of the effect of the convergent section shape on the value of F for h = 7 mm

h=7	AVR [kN]	Min. [kN]	Max. [kN]	Q25 [kN]	Q50 [kN]	Q75 [kN]
CC	33.99	32.83	34. 72	33.77	34.05	34.50
CS	31.07	27.67	36.06	27.82	30.80	33.08
CCS	24.37	21.04	28.20	23.70	23.89	25.69

by the value of p below 0.05 was applied in all the performed one-way comparisons. The null hypotheses were verified before ANOVA. First Shapiro-Wilk test was applied to check normality of the data in the populations. The value of p varied between 0.0593 and 0.7401. With this value, all the test samples were found to have Gaussian distribution. In the next step, the equality of variances was checked between the compared populations. The statistical significance p ranged 0.0501 to 0.8055 thus rejecting the null hypothesis of homogeneity of variance in the respective samples. This allowed verification of the statistical significance value with the use of the respective samples and their populations. The values of p were smaller than 0.01 for the respective groups, this confirming statistical significance of differences between the populations. The p-value details for the respective populations are given in the Tables 2-7 and the key descriptive statistics are given in Tables 8-13.

The results given in the tables indicate statistically significant differences between the compared samples. Next regression analysis was performed using CurveExpert Professional (version 2.7.3, by Daniel G. Hyams) for the purpose of fitting the function in order to describe the effect of the convergent section length and type of the F_C^{max} value. With the convergent section type being the variable, the total inside surface area of the section was determined for regression purposes. To this end, the nominal variables CC, CS and CCS were converted to ratio variables per mm^2. In most of the derived functions, linear function was used as the reference value and another non-linear function was used to obtain higher R correlation and R^2 goodness-of-fit values. The derived functions accompanied by parameters are given in Table 14 and represented by diagrams in Figure 10.

The obtained coefficient of the determination (R^2) values show that Hoerl function yielded high goodness-of-it level in most cases. In the case of

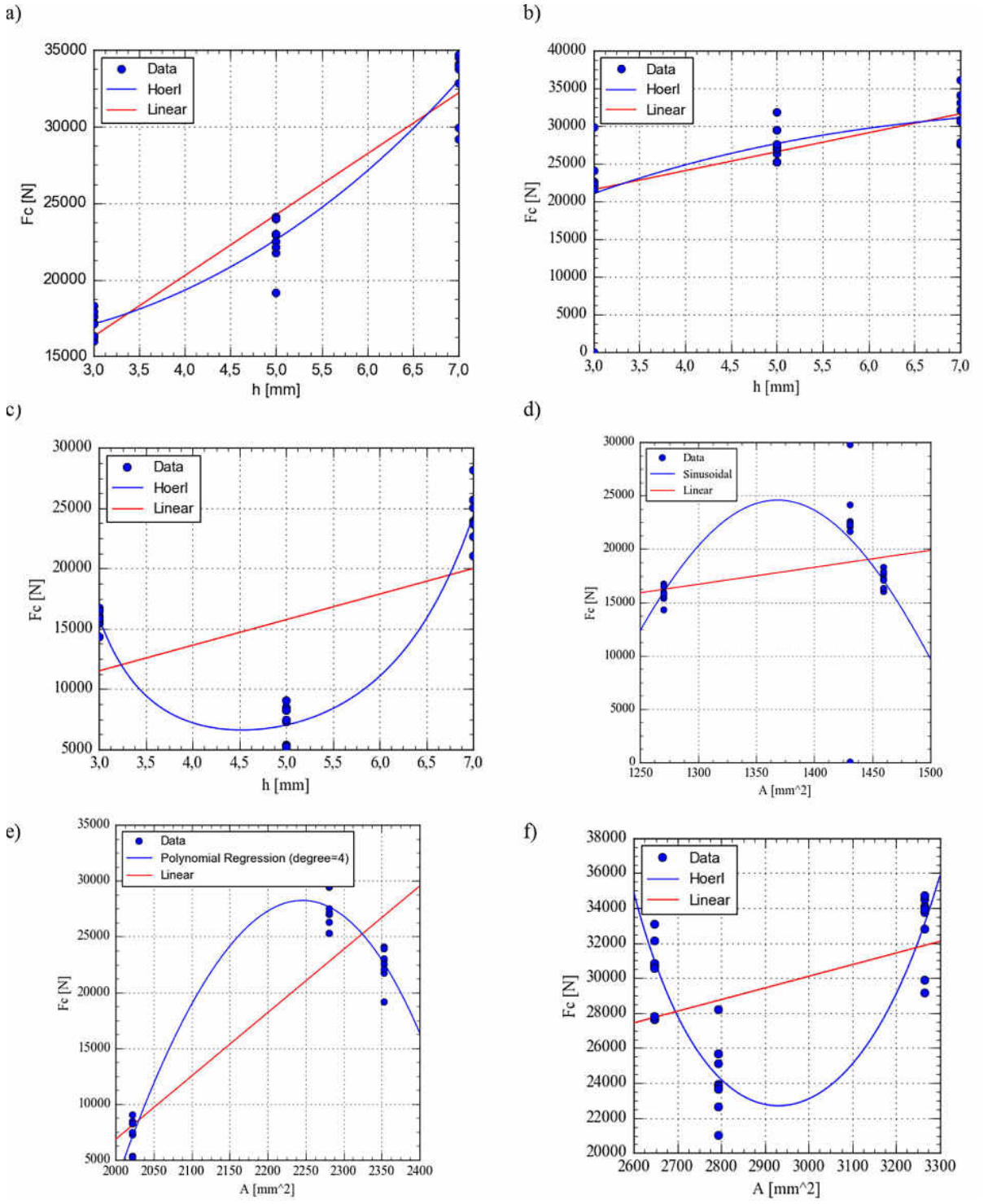

Figure 10. Regression curves for the respective data samples (a). f(*h*) for CC shaped cavity; (b) f(*h*) for CS shaped cavity; (c) f(*h*) for CCS shaped cavity, (d) f(*A*) for convergent sections of *h*=3; (e) f(*A*) for convergent sections of *h*=5; (f) f(*A*) for convergent sections of *h*=7

the sample used to estimate the change of F_C^{max} as a function of the h = 5 mm convergent section surface area the program could not determine the function factors, and hence regressions were carried out using a fourth degree polynomial. For the samples used for estimating the effect of h on the value of F_C^{max} we see that h has a linear effect on F_C^{max} in the case of CC and CS shaped cavities. Such linear relationship was not found for CCS of h = 5 data.

The same applies to the effect of the convergent section surface area on the value of F_C^{max}.

Table 14. Regression function parameters with a correlation and goodness of fit values, R – Pearson correlation coefficient, R^2 – coefficient of the determination

Parameter	Description	Function	R	R^2
F_C^{max}(CC,h)	Linear	$4.38 \cdot 10^3 + 3.973 \cdot 10^3 \cdot h$	0.9615	0.9245
	Hoerl	$1.35 \cdot 10^4 \cdot 1.329h \cdot h^{-5.67}$	0.9765	0.9536
F_C^{max}(CS,h)	Linear	$1.4 \cdot 10^4 + 2.51 \cdot 10^3 \cdot h$	0.6557	0.4300
	Hoerl	$1.03 \cdot 10^4 \cdot 0.91^h \cdot h^{0.91}$	0.6670	0.4450
F_C^{max}(CCS,h)	Linear	$5.13 \cdot 10^3 + 2.12 \cdot 10^3 \cdot h$	0.4797	0.2301
	Hoerl	$2.78 \cdot 10^6 \cdot 13.69^h \cdot h^{-11.85}$	0.9807	0.9617
F_C^{max}(h=3,A)	Linear	$-3.99 \cdot 10^3 + 15.91 \cdot h$	0.2723	0.0741
	Sinusoidal	$-3.04 \cdot 10^3 + 2.76 \cdot 10^3 \cdot \cos(8.29 \cdot 10^{-3} \cdot h + 1.22)$	0.4551	0.2071
F_C^{max}(h=5,A)	Linear	$-1.07 \cdot 10^5 + 56.7 \cdot h$	0.8907	0.7934
	Polynomial	$-6.9 \cdot 10^5 + 1.92 \cdot 10^2 \cdot h + 0.13 \cdot h^2 + 2.2 \cdot 10^{-5} \cdot h^3 - 2.47 \cdot 10^{-8} \cdot h^4$	0.9833	0.9668
F_C^{max}(h=7,A)	Linear	$1.02 \cdot 10^4 + 6.65 \cdot h$	0.3997	0.1598
	Hoerla	$1.16 \cdot 10^{193} \cdot 1.02^h \cdot h^{-62.22}$	0.8597	0.7391

Thus, it may be appropriate to test each convergent section type in parallel.

CONCLUSIONS

The output of the experimental study presented in this article is of simplified nature and concern a limited group of the extrusion die geometric features. Nonetheless, the results have confirmed the effect of the geometric features on the ultimate compression force value. This, in turn, is directly related to the extrudate density, considered the best end-product quality indicator.

Test results confirm that the type of shape and geometric parameters of channels influence the limit value of force required for extruding dry ice. Regression studies demonstrate that the height of the convergent section exhibits a nearly linear characteristic in almost all cases. In the authors' opinion, the nonlinear influence of the surface area suggests that these parameters should not be considered in future research. It can be noted, however, that in the case of research on multi-channel dies, no research results have been published so far regarding the influence of the geometric parameters of the shape of the input tapered cross-section on the value of the force boundary in the process. In this case, the studies to come shall be extended by investigation of the effect of the other geometrical features, including die cavity layout pattern, inlet diameter.

In addition, numerical analysis should be applied in further studies, to obtain more refined information on multiple-cavity die parameters ensuring optimum efficiency of the dry ice production process. As a final effect, this will allow reduction of electricity consumption and decreasing the material sublimation rate. The primary overall benefit would be improved cost efficiency of dry ice application in cooling goods in transit.

Acknowledgements

This research is a part of the project: "Developing an innovative method using the evolutionary technique to design a shaping dies used in the extrusion process of crystallized CO_2 to reduced consumption of electricity and raw material", number: "LIDER/3/0006/L-11/19/NCBR/2020" financed by National Centre for Research and Development in Poland, https://www.gov.pl/web/ncbr (accessed on: 15 December 2021).

REFERENCES

1. Kis, Z. Stability Modelling of MRNA Vaccine Quality Based on Temperature Monitoring throught the Distribution Chain, Pharmaceutics, 2022, 14(2), https://doi.org/10.3390/pharmaceutics14020430
2. Dzido, A.; Krawczyk, P.; Badyda, K.; Chondrokostas, P. Operational characteristics impact on the performance of dry-ice blasting nozzle. Energy 2021, 214, 118847. https://doi.org/10.1016/j.energy.2020.118847.
3. Górecki, J.; Wałęsa, K. and Biszczanik, A. Determination of the density of solid carbon dioxide using the hydrostatic method. AIP Conference Proceedings,

2023, http://dx.doi.org/10.1063/5.0172786

4. Spur G., Uhlmann E., Elbing F., Dry-ice blasting for cleaning: process, optimization and application. Wear, 1999, 233–235, https://doi.org/10.1016/S0043-1648(99)00204-5
5. Górecki, J., Development of a testing station for empirical verification of the algebraic model of dry ice piston extrusion. Acta Mechanica et Automatica, 2019
6. Wałęsa, K.; Górecki, J.; Berdychowski, M.; Biszczanik, A. and Wojtkowiak, D., Modelling of the Process of Extrusion of Dry Ice through a Single-Hole Die Using the Smoothed Particle Hydrodynamics (SPH) Method. Materials 2022, 15(22), 8242-1 - 8242-23, http://dx.doi.org/10.3390/ma15228242
7. Hafner, K.; Welt, B. A. and Pelletier, W., Method for Routine Density Measurement of Sublimating Solid Carbon Dioxide (dry ice) for Cold-Chain Quality Control. Journal of Applied Packaging Research, 2022, 14(1).
8. Biszczanik, A.; Wojtkowiak, D. and Wałęsa, K. Influence of the geometric characteristics of convergent extrusion channel of die on the maximum value of compaction stress of dry ice and on the quality of the obtained pellets. AIP Conference Proceedings, 2023, https://doi.org/10.1063/5.0177929
9. Górecki, J.; Talaśka, K.; Wałęsa, K.; Wilczyński, D. and Wojtkowiak, D., Mathematical Model Describing the Influence of Geometrical Parameters of Multichannel Dies on the Limit Force of Dry Ice Extrusion Process. Materials, 2020, 13(15), http://dx.doi.org/10.3390/ma13153317
10. Wałęsa, K.; Talaśka, K.; Wilczyński, D., Designing of the electromechanical drive for automated hot plate welder using load optimization with Genetic Algorithm. Materials, 2022, 15(5), http://dx.doi.org/10.3390/ma15051787
11. Gawrońska, E.; Dyja, R.; Zych, M. and Domek, G., Selection of the Heat Transfer Coefficient Using Swarming Algorithms. Acta Mech. Et Autom.2022, 16(4), 325-339, https://doi.org/10.2478/ama-2022-0039
12. Bakhtiyari, A.N.; Wang, Z; Wang, L.; Zheng, H., A review on applications of artificial intelligence in modeling and optimization of laser beam machining. Optics & Laser Technology, 2021, 135, 106721, https://doi.org/10.1016/j.optlastec.2020.106721
13. Górecki, J.; Malujda, I. and Wilczyński, D., The influence of geometrical parameters of the forming channel on the boundary value of the axial force in the agglomeration process of dry ice. MATEC Web of Conferences, 2019, 254, 05001, https://doi.org/10.1051/matecconf/201925405001
14. Biszczanik, A.; Wałęsa, K.; Kukla, M.; Górecki, J. The Influence of Density on the Value of Young's Modulus for Dry Ice. Materials 2021, 14, 7763. https://doi.org/10.3390/ma14247763.
15. Liu, Y.; Maruyama, H.; Matsusaka, S. Agglomeration process of dry ice particles produced by expanding liquid carbon dioxide. Adv. Powder Technol. 2010, 21, 652–657. https://doi.org/10.1016/j.apt.2010.07.009
16. Biszczanik, A.; Wojtkowiak, D. and Wałęsa, K. Influence of the geometric parameters of convergent extrusion channel of die on the maximum value of compaction stress of dry ice and on the quality of the obtained pellets. AIP Conference Proceedings, 2023, 2976(1), https://doi.org/10.1063/5.0177929
17. Górecki, J.; Wiktor, Ł., Influence of Die Land Length on the Maximum Extrusion Force and Dry Ice Pellets Density in Ram Extrusion Process. Materials, 2023, 16(12), https://doi.org/10.3390/ma16124281